

Maximum Likelihood Narrowband Radar Data Segmentation and Centroid Processing

Benjamin J. Slocumb^a and William D. Blair^b

^aNumerica Corporation, PO Box 271246, Ft. Collins, CO 82527, USA

^bGeorgia Tech Research Institute, Atlanta, GA 30332, USA

ABSTRACT

Electronically scanned narrowband radar systems detect non-extended targets in one or two range cells depending on whether the object straddles the range cell boundary. For two detections, the range estimate may be refined using a fusion process. However, for scenarios with multiple closely spaced objects ambiguity exists in how many objects are present and how the range cells should be paired to produce the refined estimates. In this paper, we present a new algorithm that first segments the primitive radar measurements, and second fuses paired measurements to produce object reports used by a tracking system. The segmentation algorithm is developed by forming a hypothesis partition model for a set of consecutive range cells with detections, and then evaluating the joint likelihood function for each feasible partition of the cells into pairs or singletons. Simulation results that demonstrate the utility of the algorithm are provided using a modern missile tracking simulation environment.

Keywords: Narrowband Radar, Data Segmentation, Centroid Processing, Maximum Likelihood Estimation, Target Tracking

1. INTRODUCTION

In air and missile defense, algorithm advances are being pursued to enhance radar detection, identification, and tracking performance when tracking multiple closely spaced objects. New electronically scanned array radar systems in development use advanced signal processing to provide enhanced target resolution. With the improvements in resolution it is intended that these sensors will be able to resolve and identify multiple closely spaced objects (CSOs). However, the resolution improvements alone are not sufficient to overcome the challenges of CSO tracking, and new *data segmentation/centroid processing* (DSCP) techniques are needed. In previous papers, the authors presented an electronically scanned wideband (WB) radar DSCP algorithm¹ and a mechanically scanned (rotating) radar centroid processing algorithm.² The objective of this paper is to develop an electronically scanned narrowband (NB) radar DSCP algorithm with specific focus on the CSO scenario.

In radar systems, a distinction must be made between a *primitive measurement*, which constitutes a detection in a single range cell and its associated range-bearing-elevation parameters, and an *object measurement*, which is the report that is sent to the data association and target tracking processor. For DSCP algorithm purposes, we classify a NB radar system as one where the target extent is less than the radar range cell. A detection of the target may occur in one cell or two range cells since an object may straddle a range cell boundary. In WB radar systems, the range resolution cells are smaller than the target extent and the target will produce multiple primitive measurements across a segment of range cells (possibly not all adjacent) during a single radar dwell.

To generate the object measurement report, the radar signal processor must combine primitives. First, the primitives are parsed with a *data segmentation algorithm* into object sets. For the case of NB radar, each object set consists of one or two primitives. Then, the primitives are fused into objects with a *centroid processing algorithm*; this *fusion algorithm* computes a range centroid and refines the angle estimates. Two conditions make the DSCP algorithm development challenging. When multiple CSOs are present in the data (e.g., for high debris conditions in BMD), there is an uncertainty in the association of primitives with objects. Second, multiple objects in a single range bin cause *merged monopulse measurements*, which subsequently causes direction of arrival calculation errors and poor estimates of the measurement covariance.

Other author information: Send correspondence to Email: bjslocumb@numerica.us, Telephone: 970-419-8343; Email: dale.blair@gtri.gatech.edu, Telephone: 770-528-7934.



Figure 1: Data Segmentation/Centroid Processor algorithm input/output.

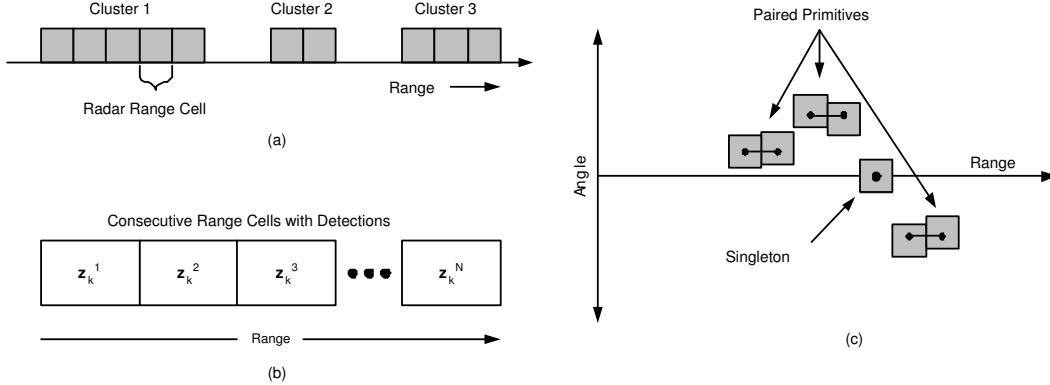


Figure 2. Diagram showing (a) separate clusters of range cells with detections in one narrowband radar dwell, (b) nomenclature for the adjacent cells, and (c) a data segmentation solution based on angular distance of adjacent cells.

This paper is organized as follows. Section 2 provides the problem formulation. Section 3 describes a probability model for the condition that a monopulse radar measurement consists of returns from two or more unresolved objects. Section 4 presents the new narrowband radar data segmentation/centroid processing algorithm. Section 5 presents simulation results, and Section 6 summarizes the paper.

2. THE NARROWBAND RADAR DSCP PROBLEM FORMULATION

The narrowband radar will make a dwell at time t_k , and in the presence multiple CSOs it will receive detections in a number of range cells. Denote $\{z_k^i; i = 1, \dots, N\}$ as the set of N primitive measurements received on the dwell, where $z_k^i = [r_k^i, b_k^i, e_k^i]^T$, i.e., the range, bearing and elevation measurements. For narrowband radar the primitive measurements from one target will always be adjacent, i.e., $r_k^i - r_k^{i-1} = \Delta r$, where Δr is the range resolution. Reported with each primitive measurement is a set of associated parameters, $\{\mathfrak{R}_{ok}^i, \sigma_{e_k^i}^2, \sigma_{b_k^i}^2, \beta_k^i, \theta_k^i\}$, where \mathfrak{R}_{ok}^i is the observed SNR, $(\sigma_{b_k^i}^2, \sigma_{e_k^i}^2)$ are the estimated bearing and elevation variances, β_k^i is the cell index, and θ_k^i represents the set of parameters provided by the monopulse merged measurement test. Range variance is not available in the primitive measurement (or is just fixed relative to the range resolution) since it consists of just one range cell. A bearing-elevation covariance \mathbf{R}_k^i may be constructed from $(\sigma_{b_k^i}^2, \sigma_{e_k^i}^2)$; depending on the system, the bearing-elevation cross correlation may be available too.

On any given radar dwell, there could be N adjacent primitive measurements. The process of converting N primitives to M objects ($N \geq M$) is shown in Figure 1. The output *object measurements* are

$$\hat{\mu}_k^j = [\hat{r}_k^j, \hat{b}_k^j, \hat{e}_k^j]^T, \quad j = 1, 2, \dots, M \quad (1)$$

These centroid estimates consist of *refined estimates* for the range, bearing and elevation and are based on the fusion of the primitives used for the j th object cluster. A covariance matrix, Σ_k^j , will also be generated for the fused measurements.

The algorithmic approach to NB radar data segmentation/centroid processing can be described as follows.

- *Form range clusters.* Candidate range clusters are identified by finding segments of primitives that could be grouped together to form a single object (see Figure 2a). For narrowband radar, a candidate cluster is a set of adjacent range

cells with active detections. A gap between active cells delineates the end of one cluster and the beginning of another cluster.

- *Apply a proximity measure.* A measure³ is applied to adjacent primitive measurements to find out how “similar” they are to each other. The distance in angle space between two primitives $(\mathbf{z}_k^i, \mathbf{z}_k^{i+1})$ identifies how closely they align, and hence their similarity. Other parameters, e.g., SNR or RCS, could also be used to identify similarity. The presence of merged monopulse measurements should be considered in the formation of the proximity measure.
- *Perform data segmentation.* Once the proximity measure of each primitive is computed, the primitives must be parsed in an “optimal way” to form object sets (one or two primitives per set). The NB radar optimization problem becomes one of determining the best pairing of primitives within a cluster such that the proximity measured is maximized over all the cells (see Figure 2c).
- *Centroid processing for object estimation.* Once the primitive measurements are parsed into objects sets, then the measurements are fused to generate the object report. The primary output of the fusion operation will be the refined estimate of the range, bearing, and elevation (RBE) of the object.

3. PROBABILITY MODEL FOR TWO OR MORE UNRESOLVED OBJECTS

3.1. Merged monopulse measurement statistical model

In this section, we form a probability model for the presence of two or more unresolved targets in one range cell. The DSCP algorithm formulated in Section 4 utilizes the probability and a merged measurement error covariance estimate developed here in the calculation of a likelihood ratio. A generalized likelihood ratio test (GLRT) for detecting the presence of two or more unresolved targets with monopulse signals was developed by Blair and Brandt-Pierce.⁴ The formulation is extended here to derive the probabilities of the presence of one resolved target or two or more unresolved targets in a given range cell via the total probability theorem. The model is formulated to use prior information from a tracking algorithm in the computation of the probabilities.

The in-phase and quadrature components of the radar sampled output of the matched filter with gain p_0 for M unresolved Rayleigh targets and subpulse* k are given by

$$s_{Ik} = \sum_{i=1}^M \alpha_{ik} \cos \psi_{ik} + n_{SIk} \quad s_{Qk} = \sum_{i=1}^M \alpha_{ik} \sin \psi_{ik} + n_{SQk} \quad (2)$$

$$d_{Ik} = \sum_{i=1}^M \eta_i \alpha_{ik} \cos \psi_{ik} + n_{dIk} \quad d_{Qk} = \sum_{i=1}^M \eta_i \alpha_{ik} \sin \psi_{ik} + n_{dQk} \quad (3)$$

where $\alpha_{ik} = \sqrt{\kappa} A_{ik} G_{\Sigma}^2(\theta_i)$, $\eta_i = G_{\Delta}(\theta_i)/G_{\Sigma}(\theta_i)$, A_{ik} is the voltage gain of target i on subpulse k with $E\{A_{ik}\} = A_{0i}$ where $E\{\cdot\}$ denotes expected value, A_{0i} is the Rayleigh parameter for the average voltage gain of target i , θ_i is the angular location of the i th target relative to antenna boresight, $G_{\Sigma}(\theta_i)$ is the antenna voltage gain of the sum channel at θ_i , $G_{\Delta}(\theta_i)$ is the antenna voltage gain of the difference channel at θ_i , and ψ_{ik} is the phase of the echo of subpulse k of target i . The sum-channel noise random variables n_{SIk} and n_{SQk} are zero-mean Gaussian with variance σ_S^2 , and difference-channel noises n_{dIk} and n_{dQk} are zero-mean Gaussian with variance σ_d^2 .

The integration of s_{Ik} and s_{Qk} from multiple pulses or subpulses is typically accomplished using the measured amplitude of the pulses and is referred to as noncoherent integration. Letting Λ_k and φ_k denote the measured amplitude and phase of the signal for subpulse k gives $s_{Ik} = \Lambda_k \cos \varphi_k$, and $s_{Qk} = \Lambda_k \sin \varphi_k$. Define the “observed SNR” for subpulse k to be $\mathfrak{R}_{ok} = \Lambda_k^2 / 2\sigma_S^2$. Since \mathfrak{R}_{ok} is actually a signal-plus-noise-to-noise ratio, the SNR of a single target is defined as $\mathfrak{R} = E\{\mathfrak{R}_{ok}\} - 1$.

The monopulse angle-of-arrival (AOA) estimation problem for target i involves the estimation of η_i and solving the inverse mapping to θ_i . In the case of a single target, the in-phase monopulse ratio is used as an estimate of η_1 . Letting

*Note for section that k is used to denote the subpulse number and that all measurements are assumed to be at the same time.

$s_k = s_{Ik} + s_{Qk}$ and $d_k = d_{Ik} + d_{Qk}$, the in-phase and quadrature monopulse ratios are given for subpulse k by

$$y_{Ik} = \operatorname{Re}\left(\frac{d_k}{s_k}\right) = \frac{d_{Ik}s_{Ik} + s_{Qk}d_{Qk}}{s_{Ik}^2 + s_{Qk}^2} \quad (4)$$

$$y_{Qk} = \operatorname{Im}\left(\frac{d_k}{s_k}\right) = \frac{d_{Qk}s_{Ik} - d_{Ik}s_{Qk}}{s_{Ik}^2 + s_{Qk}^2} \quad (5)$$

For the case of a single, isolated target and a single pulse in a conventional monopulse system, the estimate of η_1 is given by $\hat{\eta}_1 = y_{I1}$.

Let Φ_M denote the parameter set for M unresolved targets. With \Re_i denoting the average SNR for target i and $\mathcal{N}(\bar{x}, \sigma^2)$ a Gaussian distribution with mean \bar{x} and variance σ^2 , the pdf of the in-phase and quadrature parts of the monopulse ratio for subpulse k is given by

$$f(y_{Ik}, y_{Qk} | \Re_{ok}, \Phi_M) = f(y_{Ik} | \Re_{ok}, \Phi_M) f(y_{Qk} | \Re_{ok}, \Phi_M) \quad (6)$$

where

$$f(y_{Ik} | \Re_{ok}, \Phi_M) = \mathcal{N}\left(\frac{\sum_{i=1}^M \Re_i \eta_i}{\sum_{i=1}^M \Re_i + 1}, \frac{q_M}{2\Re_{ok}}\right) \quad (7)$$

$$f(y_{Qk} | \Re_{ok}, \Phi_M) = \mathcal{N}\left(0, \frac{q_M}{2\Re_{ok}}\right) \quad (8)$$

$$q_M = \left[\frac{\sigma_d^2}{\sigma_s^2} + \frac{\sum_{i=1}^M \Re_i \eta_i^2 + 0.5 \sum_{i=1}^M \sum_{j=1}^M \Re_i \Re_j (\eta_i - \eta_j)^2}{\sum_{i=1}^M \Re_i + 1} \right] \quad (9)$$

Thus, y_{Ik} and y_{Qk} are conditionally Gaussian, independent random variables. Note that (7) shows that the mean of y_I is a power or energy weighted average of the DOAs of the M targets. Also, note that the variance of the monopulse ratios increase monotonically with M since q_M increases monotonically with M . With \bar{y}_I denoting the mean of y_{Ik} given \Re_{oi} , the ML estimate of \bar{y}_I for N independent pulses is given by

$$\hat{y}_I = \frac{1}{NY_N} \sum_{k=1}^N \Re_{ok} y_{Ik}, \quad \text{where} \quad Y_N = \frac{1}{N} \sum_{k=1}^N \Re_{ok} \quad (10)$$

Since the y_{Ik} are Gaussian random variables, \hat{y}_I is the minimum variance estimate of \bar{y}_I and a Gaussian random variable with variance given by

$$\sigma_{\hat{y}_I}^2 = \frac{q_M}{2NY_N} \quad (11)$$

The modified Cramer Rao Lower Bound (MCRLB)⁵ of \bar{y}_I is given by

$$\tilde{J}_{y_I}(\bar{y}_I | N) = \frac{q_M}{2N(\sum_{i=1}^M \Re_i + 1)} \quad (12)$$

3.2. Probability of a resolved and unresolved object

The Total Probability Theorem can be used to compute the probabilities of one resolved target and two or more unresolved targets being present. These probabilities can then be used in segmenting a set of detection reports and provided to the tracker for hypothesis management. For a given range cell, let H_0 denote the hypothesis of no target, H_1 denote the hypothesis of single resolved target, and H_2 denote the hypothesis of two or more unresolved targets. Given a detection in a given range cell at time t_L , let $P\{H_0 | Z_0^L\} = 0$. Thus, using the Total Probability Theorem, the probability of one resolved target at time t_L given data Z_0^L from time t_0 through time t_L is given by

$$P\{H_1|Z_0^L\} = \frac{\prod_{k=1}^N f(y_{Ik}, y_{Qk}|\mathfrak{R}_{ok}, H_1)P\{H_1|Z_0^{L-1}\}}{\prod_{k=1}^N f(y_{Ik}, y_{Qk}|\mathfrak{R}_{ok}, H_1)P\{H_1|Z_0^{L-1}\} + \prod_{k=1}^N f(y_{Ik}, y_{Qk}|\mathfrak{R}_{ok}, H_2)P\{H_2|Z_0^{L-1}\}} \quad (13)$$

Then,

$$P\{H_2|Z_0^L\} = 1 - P\{H_1|Z_0^L\} \quad (14)$$

The unknown q_1 for H_1 can be estimated from the monopulse signals, while q_2 for H_2 needs to be estimated from *a priori* assumptions or the target state estimates. The prior probabilities $P\{H_i|Z_0^{L-1}\}$ can be derived from the target state estimates from the tracker or set uniform across all hypotheses. The prior probabilities can also be derived from a Markov chain that characterizes the switches in the number of objects to track.

As indicated by (9), the variance the monopulse ratios increase monotonically with the number of unresolved targets. Thus, q_2 characterizes a lower bound on the variance of the monopulse ratios for two or more unresolved targets and it will be used for the detection of the presence of two or more unresolved targets.

Using (6), equation (13) is reformulated to maximize the likelihood,

$$P\{H_1|Z_0^L\} = \frac{P\{H_1|Z_0^{L-1}\}}{P\{H_1|Z_0^{L-1}\} + \left(\frac{q_2}{q_1}\right)^N \exp\left(-\frac{1}{2}\frac{(q_2-q_1)}{q_1 q_2} T_N\right) P\{H_2|Z_0^{L-1}\}} \quad (15)$$

where $T_N = X_N^T R_N X_N$, and

$$X_N = [y_{I1} - \hat{y}_I \quad \dots \quad y_{IN} - \hat{y}_I \quad y_{Q1} \quad \dots \quad y_{QN}]^T \quad (16)$$

$$R_N = 2 \text{diag} [\mathfrak{R}_{o1} \quad \dots \quad \mathfrak{R}_{oN} \quad \mathfrak{R}_{o1} \quad \dots \quad \mathfrak{R}_{oN}] \quad (17)$$

If the target state estimates are not available for estimating q_2 , then some *a priori* assumptions are needed to formulate an estimate of q_2 that is useful for algorithm design and tuning. In basic form,

$$q_2 = \frac{\sigma_d^2}{\sigma_S^2} + \frac{\mathfrak{R}_1 \eta_1^2 + \mathfrak{R}_2 \eta_2^2 + \mathfrak{R}_1 \mathfrak{R}_2 (\eta_1 - \eta_2)^2}{\mathfrak{R}_1 + \mathfrak{R}_2 + 1} \quad (18)$$

and the angle variance (in radar sine space) is

$$\sigma_\theta^2 = \frac{\Theta^2 q_2}{2N Y_N k_m^2} \quad (19)$$

where Θ is the radar beamwidth and k_m is the monopulse slope.

While (18) can be estimated directly with feedback from the track filter to inflate the measurement variance for presence of unresolved targets, a simpler form is needed for the case when tracker feedback is not available. Thus, letting $\mathfrak{R}_T = \mathfrak{R}_1 + \mathfrak{R}_2$ and $\Delta\eta = \eta_2 - \eta_1$ gives

$$q_2 = \frac{\sigma_d^2}{\sigma_S^2} + \frac{\mathfrak{R}_1 \eta_1^2 + (\mathfrak{R}_T - \mathfrak{R}_1) \eta_2^2 + \mathfrak{R}_1 (\mathfrak{R}_T - \mathfrak{R}_1) (\Delta\eta)^2}{\mathfrak{R}_T + 1} \quad (20)$$

Given $\Delta\eta$, q_2 is maximized by letting $\mathfrak{R}_1 = \mathfrak{R}_2 = 0.5\mathfrak{R}_T$. Thus,

$$q_2^{max} = \frac{\sigma_d^2}{\sigma_S^2} + \frac{\mathfrak{R}_T}{2(\mathfrak{R}_T + 1)} (\eta_1^2 + \eta_2^2) + \frac{\mathfrak{R}_T^2}{4(\mathfrak{R}_T + 1)} \Delta\eta^2 \quad (21)$$

$$\approx \frac{\sigma_d^2}{\sigma_S^2} + \frac{1}{2} (\eta_1^2 + \eta_2^2) + \frac{1}{4} \mathfrak{R}_T \Delta\eta^2 \quad (22)$$

Since \bar{y}_I is a power weighted average of η_1 and η_2 , and η_i is typically less than one,

$$q_2^{max} \approx \frac{\sigma_d^2}{\sigma_S^2} + \bar{y}_I^2 + \frac{1}{4} \mathfrak{R}_T \Delta\eta^2 \quad (23)$$

where we use the approximation $\Delta\eta = 0.8$.

3.3. Prior probabilities

With respect to the computation of $P\{H_0|Z_0^{L-1}\}$, $P\{H_1|Z_0^{L-1}\}$, and $P\{H_2|Z_0^{L-1}\}$, let $\{X_{L|L-1}^j, P_{L|L-1}^j\}_{j=1}^{M_L}$ be sufficient statistics for M_L tracks, where $X_{L|L-1}^j$ and $P_{L|L-1}^j$ denote the mean and covariance for track j , respectively. In other words, let

$$P\{H_i|Z_0^{L-1}\} = P\{H_i|\{X_{L|L-1}^j, P_{L|L-1}^j\}_{j=1}^{M_L}\} \quad (24)$$

Let r_L^j denote the range random variable for track j at time L , $r_{L|L-1}^j$ denote the predicted range for track j at time L , and let $\sigma_{L|L-1}^j$ denote the standard deviation of the predicted range of track j at time L . Let $T_{j(i)}$ denote the event that track j is in range cell i . Then the probability of $T_{j(i)}$ is given by

$$P\{T_{j(i)}|Z_0^{L-1}\} = G\left(\frac{r_{(i+1)} - 0.5\Delta_r - r_{L|L-1}^j}{\sigma_{L|L-1}^j}\right) - G\left(\frac{r_{(i)} - 0.5\Delta_r - r_{L|L-1}^j}{\sigma_{L|L-1}^j}\right) \quad (25)$$

where $G(\cdot)$ is the cumulative distribution of the standard Gaussian random variable (i.e., $\mathcal{N}(0, 1)$), $r_{(i)}$ denotes the range of the center of cell i , and Δ_r denotes the range resolution of the waveform.

The Total Probability Theorem for the prior probabilities gives

$$P\{H_0|Z_0^{L-1}\} + P\{H_1|Z_0^{L-1}\} + P\{H_2|Z_0^{L-1}\} = 1 \quad (26)$$

where H_0 denotes the hypothesis that no target is present range cell under test. Then for the i th cell and M_L tracks,

$$P\{H_0|Z_0^{L-1}\} = \prod_{j=1}^{M_L} (1 - P\{T_{j(i)}|Z_0^{L-1}\}) \quad (27)$$

Also,

$$P\{H_1|Z_0^{L-1}\} = \sum_{j=1}^{M_L} P\{T_{j(i)}|Z_0^{L-1}\} \prod_{k \in I_j(M_L)} (1 - P\{T_{k(i)}|Z_0^{L-1}\}) \quad (28)$$

$$P\{H_2|Z_0^{L-1}\} = 1 - P\{H_0|Z_0^{L-1}\} - P\{H_1|Z_0^{L-1}\} \quad (29)$$

where $I_j(M_L) = \{1, 2, \dots, M_L\} \setminus j$.

4. NB RADAR DATA SEGMENTATION/CENTROID PROCESSING ALGORITHM

4.1. Formulation of hypothesis cases

We develop the DSCP algorithm by forming a hypothesis partition model for a set of consecutive range cells with detections, evaluating the joint likelihood function for each feasible partition of the cells into pairs or singletons, then performing centroid processing on the optimal partition solution. This partition approach was conceived as an extension of the methodology^{6,7} developed for detecting range-gate-pull-off false targets, where one seeks to detect the alignment of a target and a false target.

As shown in Figure 2c, the objective in the segmentation process is to identify pairs of adjacent primitive measurements that result from a single object. Each cluster of consecutive active cells (e.g, clusters 1, 2, and 3 in Figure 2a) is processed by the algorithm to partition the *primitive measurements*, \mathbf{z}_k^i , into *object measurements*, μ_k^j , which are reported to the tracking system. If a pair of primitive measurements do come from the same object, then the bearing and elevation angles should be similar. Hence, the partition problem is the find *pairs of common angle measurements* within each set of range-cell contiguous primitive measurements.

The hypothesis that a common-angle measurement pair exists is based on the bearing and elevation differences of two adjacent measurements,

$$\Delta b_k^{ij} = b_k^i - b_k^j, \quad \Delta e_k^{ij} = e_k^i - e_k^j, \quad j = i \pm 1 \quad (30)$$

In CSO scenarios, there are four possibilities (hypotheses) for the *common-angle measurements*: a same-target measurement pair, i.e., the measurements in the two bins come from the same object; a pure clutter pair; a clutter and target measurement pair; and a different-target measurement pair, i.e., the measurements in the two bins are from (at least) two different objects. In this treatment, we will focus only on the same-target and different-target hypotheses. If a measurement is from clutter (or a false alarm), then the different-target hypothesis will handle this case; however, a more rigorous statistical model^{6,7} could be applied in a future extension of the algorithm.

Table 1: Hypothesis cases for the merged measurement data segmentation centroid processing problem.

Hypothesis	Condition
$\mathbf{H}_k^{ij} = 0$	hypothesis that $(\mathbf{z}_k^i, \mathbf{z}_k^j)$ does <i>not</i> form a single-target measurement pair
$\mathbf{H}_k^{ij} = 1$	hypothesis that $(\mathbf{z}_k^i, \mathbf{z}_k^j)$ <i>does</i> form a single-target measurement pair
$\mathbf{A}_k^i = 0$	hypothesis that \mathbf{z}_k^i is a singleton, i.e., $\mathbf{H}_k^{i-1,i} = 0$ and $\mathbf{H}_k^{i,i+1} = 0$
$\mathbf{A}_k^i = 1$	hypothesis that \mathbf{z}_k^i is paired with \mathbf{z}_k^{i-1} , i.e., $\mathbf{H}_k^{i-1,i} = 1$ and $\mathbf{H}_k^{i,i+1} = 0$
$\mathbf{A}_k^i = 2$	hypothesis that \mathbf{z}_k^i is paired with \mathbf{z}_k^{i+1} , i.e., $\mathbf{H}_k^{i-1,i} = 0$ and $\mathbf{H}_k^{i,i+1} = 1$
$\mathbf{A}_k^i = 3$	hypothesis that \mathbf{z}_k^i is paired with \mathbf{z}_k^{i-1} and \mathbf{z}_k^{i+1} , i.e., $\mathbf{H}_k^{i-1,i} = 1$ and $\mathbf{H}_k^{i,i+1} = 1$
$\mathbf{M}_k^i = 0$	hypothesis that \mathbf{z}_k^i is <i>not</i> a merged measurement
$\mathbf{M}_k^i = 1$	hypothesis that \mathbf{z}_k^i <i>is</i> a merged measurement

We use \mathbf{H}_k^{ij} to denote the *pairing hypothesis* of the measurements \mathbf{z}_k^i and \mathbf{z}_k^j . We also use \mathbf{M}_k^i to denote the *merged measurement hypothesis* of \mathbf{z}_k^i . Table 1 summarizes the definition of the hypotheses. With these definitions, the conditional density functions given the pairing hypotheses are defined as

$$f(\Delta b_k^{ij}, \Delta e_k^{ij} | \mathbf{H}_k^{ij} = 1) = f_{t1}(\Delta b_k^{ij}, \Delta e_k^{ij}) \quad (31)$$

$$f(\Delta b_k^{ij}, \Delta e_k^{ij} | \mathbf{H}_k^{ij} = 0) = f_{t2}(\Delta b_k^{ij}, \Delta e_k^{ij}) \quad (32)$$

where $t1$ refers to a single target and $t2$ refers to two or more different targets. These two density functions are defined in Section 4.2. We use \mathbf{A}_k^i to represent another hypothesis regarding measurement \mathbf{z}_k^i . This hypothesis combines the pairing hypotheses for $(\mathbf{z}_k^{i-1}, \mathbf{z}_k^i)$ and $(\mathbf{z}_k^i, \mathbf{z}_k^{i+1})$. In Table 1, we define the four possible values of this hypothesis. When \mathbf{A}_k^i takes one of these values, constraints will result on the allowable value of the neighbor hypotheses \mathbf{A}_k^{i-1} and \mathbf{A}_k^{i+1} . For each case of \mathbf{A}_k^i , the allowable values of \mathbf{A}_k^{i-1} and \mathbf{A}_k^{i+1} are shown in Table 2. These constraints arise because one pairing hypothesis for one measurement eliminates the potential pairing with another measurement.

4.2. Density functions for measurement pairs

4.2.1. Statistical models for angle measurements

The bearing of a target measurement, b_k^i , has a Gaussian distribution with mean θ_k^t and variance $\hat{\sigma}_{b_k^i}^2$. Here, θ_k^t is the true bearing to the target. The bearing variance is the measurement variance estimated by the radar signal processor using the monopulse voltages in the sum and difference channels produce by the target return. The elevation measurement of the

Table 2: Constraints on the \mathbf{A}_k^i hypotheses.

Case	Allowable values of \mathbf{A}_k^{i-1}	Allowable values of \mathbf{A}_k^{i+1}
$\mathbf{A}_k^i = 0$	0,1	0,2
$\mathbf{A}_k^i = 1$	2,3	0,2
$\mathbf{A}_k^i = 2$	0,1	1,3
$\mathbf{A}_k^i = 3$	2,3	1,3
Not allowed: $\mathbf{A}_k^1 \neq 1, 3$ and $\mathbf{A}_k^N \neq 2, 3$		

target follows an identical statistical model, $e_k^i \sim \mathcal{N}(\phi_k^t, \hat{\sigma}_{e_k^i}^2)$, with ϕ_k^t being the true elevation to the target and $\hat{\sigma}_{e_k^i}^2$ being the estimated elevation variance produced by the radar signal processor.

The statistical model of the angle measurements actually has two separate cases. One case is for when there is only a single object in the cell (i.e., no merged measurements). The other case is for when two or more objects exist in the cell (i.e., merged measurements). Under the two cases, the measurement variance will be different,

$$\mathbf{M}_k^i = 0 \quad : \quad (\hat{\sigma}_{b_k^i}^2, \hat{\sigma}_{e_k^i}^2) \equiv (\hat{\sigma}_{b_k^i(0)}^2, \hat{\sigma}_{e_k^i(0)}^2) \quad (33)$$

$$\mathbf{M}_k^i = 1 \quad : \quad (\hat{\sigma}_{b_k^i}^2, \hat{\sigma}_{e_k^i}^2) \equiv (\hat{\sigma}_{b_k^i(1)}^2, \hat{\sigma}_{e_k^i(1)}^2) \quad (34)$$

The merged measurement variance estimates $(\hat{\sigma}_{b_k^i(1)}^2, \hat{\sigma}_{e_k^i(1)}^2)$ are not the values returned by the radar signal processor and are instead produced by a separate variance estimator shown in (19).

4.2.2. Density function for a same-target pair

Hypothesis $\mathbf{H}_k^{ij} = 1$ implies that \mathbf{z}_k^i and \mathbf{z}_k^j originate from the same target and have common bearing and elevation angles. Hence, the mean value of the angle differences is zero because $E\{b_k^i\} - E\{b_k^j\} = \theta_k^t - \theta_k^t = 0$ and $E\{e_k^i\} - E\{e_k^j\} = \phi_k^t - \phi_k^t = 0$. The value of the variance depends on whether a merged measurement is assumed and we condition the density on both possibilities for each range cell,

$$\begin{aligned} f_{t1}(\Delta b_k^{ij}, \Delta e_k^{ij} | \mathbf{M}_k^i = m_i, \mathbf{M}_k^j = m_j) &= \mathcal{N}(\Delta b_k^{ij}; 0, \hat{\sigma}_{b_k^i(m_i)}^2 + \hat{\sigma}_{b_k^j(m_j)}^2) \\ &\times \mathcal{N}(\Delta e_k^{ij}; 0, \hat{\sigma}_{e_k^i(m_i)}^2 + \hat{\sigma}_{e_k^j(m_j)}^2), \quad m_i, m_j \in \{0, 1\} \end{aligned} \quad (35)$$

The unconditional density function for a same-target pair is obtained by summing over the probabilities for each merged measurement hypothesis,

$$f_{t1}(\Delta b_k^{ij}, \Delta e_k^{ij}) = \sum_{m_i=0}^1 \sum_{m_j=0}^1 f_{t1}(\Delta b_k^{ij}, \Delta e_k^{ij} | \mathbf{M}_k^i = m_i, \mathbf{M}_k^j = m_j) \cdot \Pr\{\mathbf{M}_k^i = m_i\} \cdot \Pr\{\mathbf{M}_k^j = m_j\} \quad (36)$$

where $\Pr\{\mathbf{M}_k^i = 1\}$ is the probability that \mathbf{z}_k^i is a merged measurement and $\Pr\{\mathbf{M}_k^i = 0\}$ is the probability it is not a merged measurement. These probability values were derived in (14) and (15) and can incorporate the feedback state data from the tracker.

4.2.3. Density function for a different-target pair

Hypothesis $\mathbf{H}_k^{ij} = 0$ implies that \mathbf{z}_k^i and \mathbf{z}_k^j originate from two different targets[†] and therefore have different bearing and elevation angles. Hence, this hypothesis implies that $E\{\Delta b_k^{ij}\} \neq 0$ and $E\{\Delta e_k^{ij}\} \neq 0$. To model this situation, we have created an inverted Gaussian density function with the characteristics shown in Figure 3. The bell width of this inverted Gaussian is the same as for the same target case shown in (36); thus it matches the uncertainty profile. Mathematically, this density function is defined as follows,

$$f_{t2}(\Delta b_k^{ij}, \Delta e_k^{ij} | \mathbf{M}_k^i = m_i, \mathbf{M}_k^j = m_j) = \frac{1}{c_b} \left(1 + \epsilon - \exp \left(\frac{-(\Delta b_k^{ij})^2}{2(\hat{\sigma}_{b_k^i(m_i)}^2 + \hat{\sigma}_{b_k^j(m_j)}^2)} \right) \right) \quad (37)$$

$$\times \frac{1}{c_e} \left(1 + \epsilon - \exp \left(\frac{-(\Delta e_k^{ij})^2}{2(\hat{\sigma}_{e_k^i(m_i)}^2 + \hat{\sigma}_{e_k^j(m_j)}^2)} \right) \right) \quad (38)$$

where $m_i, m_j \in \{0, 1\}$, and the parameter ϵ is a tuning parameter used to define the density value at (0,0). Two normalization parameters are defined as follows,

$$c_b = 2\Theta_b(1 + \epsilon) - \sqrt{2\pi}(\hat{\sigma}_{b_k^i(m_i)}^2 + \hat{\sigma}_{b_k^j(m_j)}^2) \operatorname{erf} \left(\frac{\sqrt{2}\Theta_b}{2(\hat{\sigma}_{b_k^i(m_i)}^2 + \hat{\sigma}_{b_k^j(m_j)}^2)} \right) \quad (39)$$

[†]This hypothesis also covers the case of a target and clutter, or clutter and clutter.

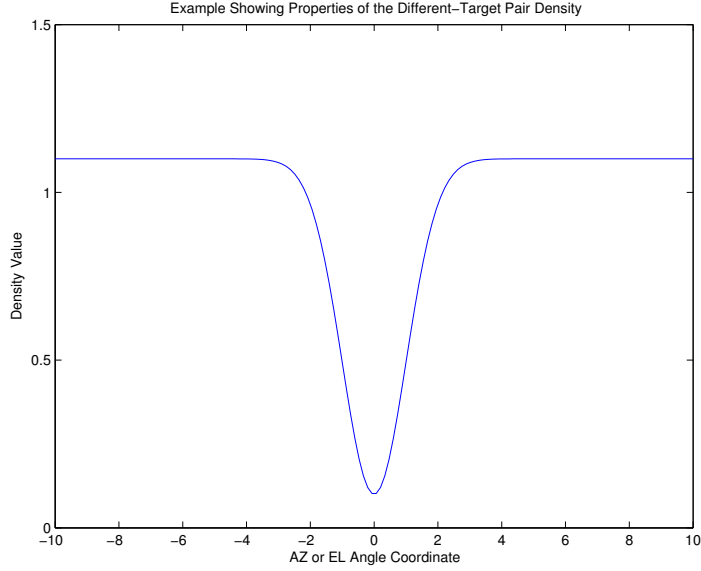


Figure 3: Plot showing the properties of the defined inverted Gaussian density.

$$c_e = 2\Theta_e(1 + \epsilon) - \sqrt{2\pi}(\hat{\sigma}_{e_k^i(m_i)}^2 + \hat{\sigma}_{e_k^j(m_j)}^2) \operatorname{erf}\left(\frac{\sqrt{2}\Theta_e}{2(\hat{\sigma}_{e_k^i(m_i)}^2 + \hat{\sigma}_{e_k^j(m_j)}^2)}\right) \quad (40)$$

Here, Θ_b is the radar bearing beamwidth, and Θ_e is the elevation beamwidth. In deriving (c_b, c_e) we assume that $-\Theta_b < \Delta b_k^{ij} < \Theta_b$ and $-\Theta_e < \Delta e_k^{ij} < \Theta_e$, i.e., the separation in angle is at most one beamwidth. Technically, the density in (41) should be defined as zero outside $[-\Theta_b, \Theta_b]$ and $[-\Theta_e, \Theta_e]$, but since this happens with such small frequency, we let the density evaluate to its asymptotic value (the desired effect since we want the density to be large when the angle difference between the cells is large).

Finally, the unconditional density for the different-target case is obtained using the probabilities for merged measurements in each cell,

$$f_{t2}(\Delta b_k^{ij}, \Delta e_k^{ij}) = \sum_{m_i=0}^1 \sum_{m_j=0}^1 f_{t2}(\Delta b_k^{ij}, \Delta e_k^{ij} | \mathbf{M}_k^i = m_i, \mathbf{M}_k^j = m_j) \cdot \Pr\{\mathbf{M}_k^i = m_i\} \cdot \Pr\{\mathbf{M}_k^j = m_j\} \quad (41)$$

4.3. Partition algorithm for data segmentation

4.3.1. Maximum likelihood approach

To assess whether a pair of measurements belong to the same target, (i.e., have the same bearing and elevation), we form the likelihood function for each of the hypotheses $\mathbf{H}_k^{ij} = 1$ and $\mathbf{H}_k^{ij} = 0$,

$$L_k^{ij}(1) = f(\Delta b_k^{ij}, \Delta e_k^{ij} | \mathbf{H}_k^{ij} = 1) = f_{t1}(\Delta b_k^{ij}, \Delta e_k^{ij}) \quad (42)$$

$$L_k^{ij}(0) = f(\Delta b_k^{ij}, \Delta e_k^{ij} | \mathbf{H}_k^{ij} = 0) = f_{t2}(\Delta b_k^{ij}, \Delta e_k^{ij}) \quad (43)$$

where f_{t1} is taken from (36) and f_{t2} is taken from (41). By computing the likelihood function for both hypotheses, $L_k^{ij}(0)$ and $L_k^{ij}(1)$, one can find the *maximum likelihood hypothesis* for the pair of measurements (i.e., this is the maximum likelihood approach).

To find the optimal partition, we form the joint likelihood function for the pairing hypotheses in the set of adjacent measurements $\{\mathbf{z}_k^1, \dots, \mathbf{z}_k^N\}$. The particular realization of hypotheses that maximizes the joint likelihood function is the

maximum likelihood estimate for the data segmentation. Recall from Table 1 that we formulated four possible hypotheses, $\mathbf{A}_k^i \in \{0, 1, 2, 3\}$, for each measurement. Let us define \mathcal{A}_{kr} to be the r th realization at time t_k of the hypotheses,

$$\mathcal{A}_{kr} = \{\mathbf{A}_k^1 = a_{kr}^1, \dots, \mathbf{A}_k^N = a_{kr}^N\}, \quad a_{kr}^i \in \{0, 1, 2, 3\} \quad (44)$$

Now define another likelihood function for the i th measurement that determines its value based on the defined partition,

$$\ell_k^i(\mathcal{A}_{kr}) = \begin{cases} L_k^{i,i+1}(1), & \text{if } a_{kr}^i \in \{2, 3\}, \text{ and } a_{kr}^{i+1} \in \{1, 3\} \\ L_k^{i,i+1}(0), & \text{if } a_{kr}^i \in \{0, 1\}, \text{ and } a_{kr}^{i+1} \in \{0, 2\} \end{cases} \quad (45)$$

Then the joint likelihood function for the hypothesis realization \mathcal{A}_{kr} is

$$\Lambda(\mathcal{A}_{kr}) = \prod_{i=1}^{N-1} \ell_k^i(\mathcal{A}_{kr}) \quad (46)$$

From this joint likelihood function the optimal partition of the measurements is the hypothesis partition \mathcal{A}_{kr^*} , where the realization r^* is determined by

$$r^* \leftarrow \arg \max_r \Lambda(\mathcal{A}_{kr}) \quad (47)$$

4.3.2. Partition enumeration and validity checking

To find the optimal partition at time t_k , one must enumerate the all the possible pairing hypotheses, \mathcal{A}_{kr} , $r = 1, 2, \dots$, and compute associated joint likelihood $\Lambda(\mathcal{A}_{kr})$. Within the enumeration of the pairing hypotheses, we must check to see if the hypotheses are valid based on the constraints shown in Table 2 for allowable values of \mathbf{A}_k^i . The general outline for generating the possible partitions is as follows:

1. Initialize $r = 1$, and the set the hypothesis realization $\mathcal{A}_1 = \{a_{kr}^1 = 0, a_{kr}^2 = 0, \dots, a_{kr}^N = 0\}$.
2. Increment the hypothesis indices $\{a_{kr}^1, \dots, a_{kr}^N\}$ to the next feasible values, i.e., such that $a_{kr}^i \in \{0, 1, 2, 3\}$.
3. Check the validity of the hypothesis realization using the constraints shown in Table 2.
 - (a) If valid, then increment r and set \mathcal{A}_{kr} to the new realization.
 - (b) Otherwise, skip the realization.
4. Check if the end condition has been reached (i.e., all $a_{kr}^i = 3$), and if not return to step 2.

4.4. Centroid processing algorithm

Once the optimal partition of the primitive measurements has been determined from (46), then the primitives can be fused using the centroid processing algorithm. The output will be a set of *object measurements*. There are three partition cases to consider when generating the centroid output.

- Pair case: two primitive measurements have been determined to be from the same target and should be fused into a single object report.
- Singleton case: a primitive measurement has been determined not to be paired with any others and should be returned as a single object report.
- Multiple pairing case: if the i th primitive is determined to go with both the $i - 1$ and $i + 1$ primitives, then a multi-pairing solution exists and a second partition algorithm is required to generate object reports.

4.4.1. Pair case

When $(\mathbf{z}_k^i, \mathbf{z}_k^{i+1})$ is determined to be a single-target pair, then the object report is generated from the fusion of these primitive measurements. The bearing and elevation angle fusion and the range fusion are accomplished in separate steps. First, define the following auxiliary vector and covariance,

$$\mathbf{y}_k^i = [b_k^i \ e_k^i]^T \quad (48)$$

$$\Gamma_k^i = \text{cov}(\mathbf{y}_k^i) = \text{diag}[\hat{\sigma}_{b_k^i}^2, \hat{\sigma}_{e_k^i}^2] \quad (49)$$

where the bearing and elevation variances are

$$\hat{\sigma}_{b_k^i}^2 = \hat{\sigma}_{b_k^i(0)}^2 \cdot \Pr\{\mathbf{M}_k^i = 0\} + \hat{\sigma}_{b_k^i(1)}^2 \cdot \Pr\{\mathbf{M}_k^i = 1\} \quad (50)$$

$$\hat{\sigma}_{e_k^i}^2 = \hat{\sigma}_{e_k^i(0)}^2 \cdot \Pr\{\mathbf{M}_k^i = 0\} + \hat{\sigma}_{e_k^i(1)}^2 \cdot \Pr\{\mathbf{M}_k^i = 1\} \quad (51)$$

Note, bearing-elevation cross-correlation can be added if available. The bearing and elevation fusion is accomplished using the standard fusion equations,

$$\hat{\mathbf{y}}_k = \hat{\Gamma}_k \left((\Gamma_k^i)^{-1} \mathbf{y}_k^i + (\Gamma_k^{i+1})^{-1} \mathbf{y}_k^{i+1} \right) \quad (52)$$

$$\hat{\Gamma}_k = \left((\Gamma_k^i)^{-1} + (\Gamma_k^{i+1})^{-1} \right)^{-1} \quad (53)$$

If the measurements in adjacent cells are correlated, then the Linear Combination with Cross-Covariance fusion method⁸ may be used.

Meanwhile, the range fusion is computed as the SNR-weighted average of the two range cell values,

$$\hat{r}_k = \frac{\mathfrak{R}_k^i \cdot r_k^i + \mathfrak{R}_k^{i+1} \cdot r_k^{i+1}}{\mathfrak{R}_k^i + \mathfrak{R}_k^{i+1}} \quad (54)$$

The range variance is more difficult to handle. If the object is not closely spaced with other objects, then the estimate \hat{r}_k will be very accurate (in fact, through simulation it was observed to achieve the CRLB). However, if CSOs are present, then the partition uncertainty will be significantly under-represented in the range estimate. Therefore, we can use one of two values for the range variance based on a level of certainty in the assignment of the measurement to the pair,

$$\text{var}(\hat{r}_k) = \begin{cases} \Delta r^2 / 12, & \text{Association uncertain} \\ \Delta r^2 / (4 \cdot \text{SNR}), & \text{Association certain} \end{cases} \quad (55)$$

where the first definition is for ‘‘uniform’’ uncertainty across the range cell, and the second definition is the Cramer-Rao Lower Bound given a pair of measurements. Whether the association is certain or not can be determined two ways. One is to compare the optimal value of $\ell_k^i(\mathcal{A}_{kr})$ to the next best score. If $\ln(\ell_k^i(\mathcal{A}_{kr^*})/\ell_k^i(\mathcal{A}_{kr})) > \gamma$, for some threshold $\gamma \geq 0$ and next-best solution r , then we decide the assignment is certain. A second approach is to detect when $\Pr\{\mathbf{M}_k^i = 1\} > \gamma$. This implies a high probability of merged measurements (and thus nearby objects), hence the partition solution is uncertain. We used the latter approach in our simulation study.

In the final step, the j th *object measurement* report is prepared and sent to the tracker. The object position and covariance report is

$$\hat{\mu}_k^j = \begin{bmatrix} \hat{r}_k \\ \hat{\mathbf{y}}_k \end{bmatrix}, \quad \Sigma_k^j = \begin{bmatrix} \text{var}(\hat{r}_k) & \mathbf{0} \\ 0 & \hat{\Gamma}_k \end{bmatrix}, \quad j = 1, \dots, M \quad (56)$$

4.4.2. Singleton case

When \mathbf{z}_k^i is selected to be a singleton, then formation of the object measurement is trivial (the input is mapped straight to the output),

$$\hat{\mu}_k^j = \mathbf{z}_k^i = [r_k^i \ b_k^i \ e_k^i]^T \quad (57)$$

$$\Sigma_k^j = \mathbf{R}_k^i = \text{diag}[\text{var}(r_k^i), \sigma_{b_k^i}^2, \sigma_{e_k^i}^2] \quad (58)$$

Since the report is based on only a single primitive measurement, range estimation using a power-weighted average is not possible. The object lies somewhere within one range cell, and the most conservative way to estimate the range variance is $\Delta r^2/12$, i.e., assume the target location is uniform random variable over the range cell. However, this estimate of the variance can be improved as follows. Since the object was detected in only a single range cell, we know that the amount of energy in an adjacent cell (due to bin straddling) is below the detection threshold. If $(\Delta r - \epsilon)$ is the portion of the pulse in the cell, and ϵ is the portion in the adjacent cell, then the energy relation may be described as follows,

$$c(\Delta r - \epsilon)^2 = \mathfrak{R}_0 \quad (59)$$

$$c\epsilon^2 = \gamma_0 \quad (60)$$

where \mathfrak{R}_0 is the observed SNR, γ_0 is the detection threshold, and c is a constant. Then, solving these simultaneous equations for ϵ we get

$$\epsilon = \frac{(\pm\sqrt{\mathfrak{R}_0\gamma_0} - \gamma_0)\Delta r}{\mathfrak{R}_0 - \gamma_0} \quad (61)$$

Notice that ϵ converges to Δr as the SNR approaches the threshold. In essence, this estimate of ϵ gives us the worst-case fraction of the pulse that could be in an adjacent cell. Hence, it represents the maximum range uncertainty in the location of the object and the range variance should be computed as

$$\text{var}(r_k^i) = \frac{\epsilon^2}{12} \quad (62)$$

In practice it is wise to put a lower limit on ϵ to ensure that the range variance is not too small (which might cause the track covariance to collapse).

4.4.3. Multiple pairing case

If the optimal partition of the primitive data selects $\mathbf{A}_k^i = 3$ for some i , then \mathbf{z}_k^i is paired with both \mathbf{z}_k^{i-1} and \mathbf{z}_k^{i+1} . This outcome likely implies that multiple (at least two) objects are closely spaced, and that merged measurements are very possible. Given this, we need a second partition algorithm to refine the partition determined by joint likelihood maximizer of (46). Two possible approaches have been identified.

- *Minimum Object Approach.* The cells can be paired off using the assumption that a minimum number of objects is present. This logic can be automatically invoked by removing the pairing outcome $\mathbf{A}_k^i = 3$, and forcing the maximum likelihood estimator to select $\mathbf{A}_k^i \in \{0, 1, 2\}$. That is, the best pairing outcome is enforced. For the simulations in this paper, this was the approach used.
- *Multi-Object Approach.* With more refinement of the merged measurement model, it is possible to extend the joint likelihood function to allow for the estimation of the number of objects present (in addition to the partition). Further development of this approach is left for future work.

Once the second partition algorithm has been applied to the primitives, the centroid processing algorithm described in Section 4.4.1 is applied to fuse primitives and generate the object reports.

5. SIMULATION RESULTS

To evaluate the performance of the new narrowband radar data segmentation/centroid processing (DSCP) algorithm described in Section 4, a MATLAB implementation of the algorithm was completed and the algorithm was and tested within a missile tracking simulation with a CSO scenario. To score the performance of the new DSCP algorithm, we used the simulation metrics package and examined the tracking performance. By assessing the tracking performance *using a common tracking algorithm*, we examined the impact of the DSCP algorithm on the tracking performance.

Figure 4 first demonstrates the implementation of DSCP algorithm. The top graph plots the primitive measurement range versus azimuth (elevation not shown). Eight primitives were formed from nine closely spaced objects (i.e., multiple merged measurements). The DSCP algorithm formed five outputs (numbered on graph): three were formed from pairs of primitives, two were formed from singletons. The lower graph shows the SNR for each primitive, and from this one can

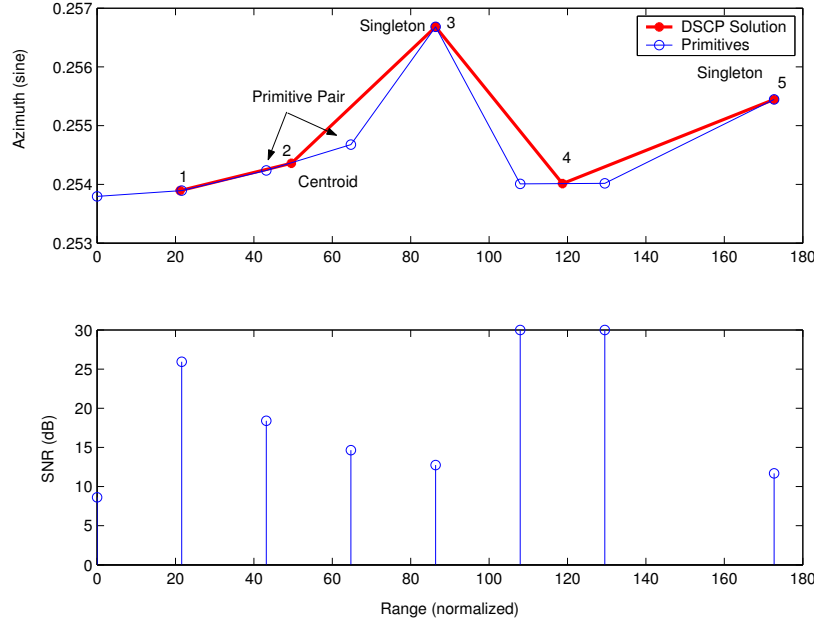


Figure 4. Demonstration of the DSCP algorithm. Top graph shows the primitives and DSCP outputs (range vs. azimuth), and lower graph shows primitive SNR vs. range.

see that the DSCP solutions formed from primitive pairs are appropriately weighted in range toward the primitive with highest SNR.

Figure 5 shows tracking performance comparison plots. The first graph shows the cumulative breaks metric, while the second graph shows the metric for the cumulative number of switches (for a particular object). In the former case, the cumulative number of breaks of tracks is computed by counting the cumulative number of track breaks up to the scoring time (for each truth object) summed across all reportable objects (and then averaged over Monte Carlo trials). The figure shows that (by time 300 sec) that there are three times as many track breaks with the Default method[‡] compared to the New DSCP method developed here. The explanation for the performance difference is that the new DSCP algorithm (i) does a better job of segmenting the measurements, and (ii) the measurement covariance matrix reported with the object report better represents the uncertainty in the data (and hence the tracker is better able to keep track). The metric for cumulative switches is computed by counting the number of times that the track number assigned to each truth object has changed. The comparison of the plots show roughly a 20% improvement in performance with the New method. Here, we postulate that the improved segmentation method ensures that tracks are better able to continue on a direct course (and thus track swapping is less likely).

6. SUMMARY

In this paper, we have formulated a new narrowband radar data segmentation/centroid processing algorithm. The approach is to form the likelihood function for the pairing of adjacent measurement. By computing the hypothesis realization that maximizes the joint likelihood function, we determine the optimal partition of the primitive measurements. Merged measurement probabilities and tracker feedback are used in the computation of variances used in the joint likelihood function. Once the optimal partition is determined, a fusion algorithm is applied to generate the centroid estimates (i.e., the object reports). Simulation results show that the methodology works well in a realistic missile tracking scenario, and the results demonstrate performance advantages over a Default methodology.

[‡]The Default method for centroid processing is one that is provided with the simulation. It uses a Chi-square angle distance to parse primitives, but then enforces a pair-wise segmentation.

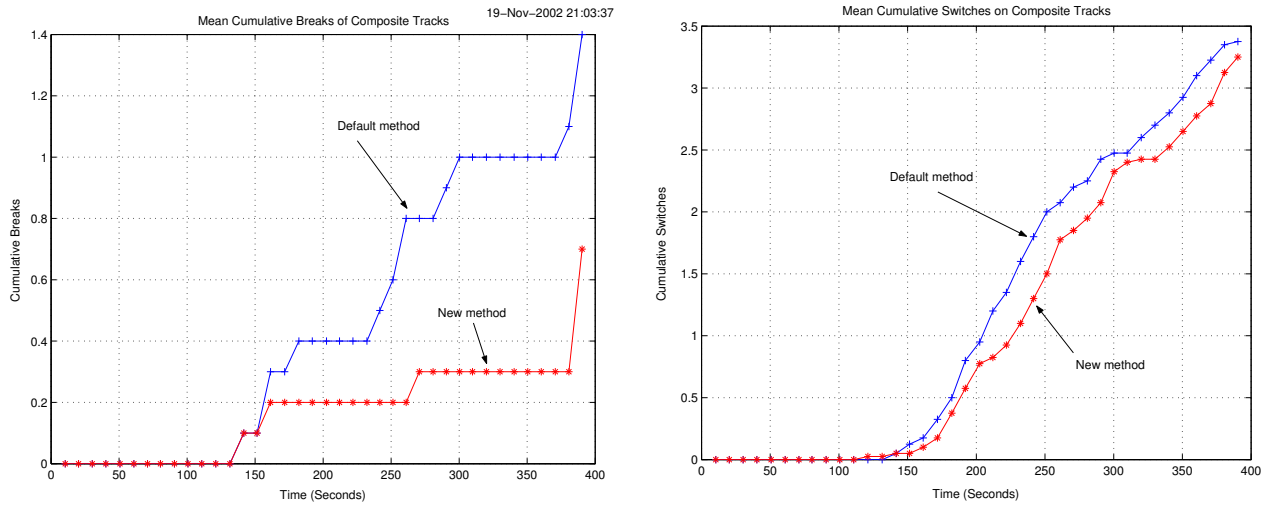


Figure 5: Cumulative breaks comparison, and cumulative switches comparison.

ACKNOWLEDGMENTS

This work was supported by MDA under contract HQ0006-02-C-0028.

REFERENCES

1. B. Slocumb and W. Blair, "EM-based measurement fusion for HRR radar centroid processing," *Proceedings of SPIE Conference on Signal and Data Processing of Small Targets* **4728**, April 2002.
2. B. J. Slocumb, "Surveillance radar range-centroid processing," *Proceedings of the SPIE, Conference on Signal and Data Processing of Small Targets* **4473**, 2001.
3. S. Theodoridis and K. Koutroumbas, *Pattern Recognition*, Academic Press, San Diego, CA, 1999.
4. W. Blair and M. Brandt-Pierce, "Unresolved rayleigh target using monopulse measurements," *IEEE Transactions on Aerospace and Electronic Systems*, pp. 543–552, April 1998.
5. W. Blair and M. Brandt-Pierce, "Monopulse doa estimation for two unresolved rayleigh targets," *IEEE Transactions on Aerospace and Electronic Systems*, pp. 452–469, April 2001.
6. X. R. Li, B. J. Slocumb, and P. D. West, "Tracking in the presence of range deception ECM and clutter by decomposition and fusion," *Proceedings of the SPIE, Conference on Signal and Data Processing of Small Targets* **3809**, pp. 198–210, July 1999.
7. B. J. Slocumb, P. D. West, and X. R. Li, "Implementation and analysis of the decomposition-fusion ECCM technique," *Proceedings of the SPIE, Conference on Signal and Data Processing of Small Targets* **4048**, pp. 486–497, April 2000.
8. Y. Bar-Shalom and L. Campo, "The effect of the common process noise on the two-sensor fused track covariance," *IEEE Transactions on Aerospace and Electronic Systems* **22**, pp. 803–805, November 1986.